

Heterologous Expression of *Pharaonis* Halorhodopsin in *Xenopus laevis* Oocytes and Electrophysiological Characterization of Its Light-Driven Cl[−] Pump Activity

Akiteru Seki,* Seiji Miyauchi,* Saori Hayashi,* Takashi Kikukawa,[†] Megumi Kubo,[‡] Makoto Demura,[‡] Vadivel Ganapathy,[§] and Naoki Kamo[‡]

*Graduate School of Pharmaceutical Sciences, [†]Laboratory of Biomolecular Systems, Creative Research Initiative “Sosei”, and

[‡]Department of Biomolecular Science, Faculty of Advanced Life Sciences, Hokkaido University, Sapporo, Japan; and

[§]Department of Biochemistry and Molecular Biology, Medical College of Georgia, Augusta, Georgia

ABSTRACT *Natronomonas pharaonis* halorhodopsin (pHR) is an archaeal rhodopsin functioning as an inward-directed, light-driven Cl[−] pump. To characterize the electrophysiological features of the Cl[−] pump activity of pHR, we expressed pHR in *Xenopus laevis* oocytes and analyzed its photoinduced Cl[−] pump activity using the two-electrode voltage-clamp technique. Photoinduced outward currents were observed only in the presence of Cl[−], Br[−], I[−], NO₃[−], and SCN[−], but not in control oocytes, indicating that photoinduced anion currents were mediated by pHR. The relationship between photoinduced Cl[−] current via pHR and the light intensity was linear, demonstrating that transport of Cl[−] is driven by a single-photon reaction and that the steady-state current is proportional to the excited pHR molecule. The current-voltage relationship for pHR-mediated photoinduced currents was also linear between −150 mV and +50 mV. The slope of the line describing the current-voltage relationship increased as the number of the excited pHR molecules was increased by the light intensity. The reversal potential (*V_R*) for Cl[−] as the substrate for the anion pump activity of pHR was about −400 mV. The value for *V_R* was independent of light intensity, meaning that the *V_R* reflects the intrinsic value of the excited pHR molecule. The value of *V_R* changed significantly for the R123K mutant of pHR. We also show that the Cl[−] pump activity of pHR can generate a substantial negative membrane potential, indicating that pHR is a very potent Cl[−] pump. We have also analyzed the kinetics of voltage-dependent Cl[−] pump activity as well as that of the photocycle. Based on these data, a kinetic model for voltage-dependent Cl[−] transport via pHR is presented.

INTRODUCTION

Halorhodopsin (HR), discovered in the archaeobacterium *Halobacterium* is an inward-directed Cl[−] pump (1–4). HR, functioning as a Cl[−] pump, has the ability to transport Cl[−] against an electrochemical gradient, and can generate an inside-negative membrane potential to support ATP synthesis (1,5,6). Since its original discovery, several HRs from different sources have been reported; but most studies focusing on the functional aspects of HR have used *Halobacterium salinarum* halorhodopsin (sHR) and *Natronomonas pharaonis* halorhodopsin (pHR) as model systems (4,7). These two proteins show high similarity in amino acid sequences (identity, 66%; homology, 97%). Based on the high sequence homology between the two Cl[−] pumps and their similar photoinduced intermediates, it has been assumed that these proteins have similar structure (8–11).

Recently, the x-ray crystal structure of sHR was determined at a resolution of 1.8 Å, and it showed striking similarity to that of bacteriorhodopsin (BR) (4,12,13). sHR is composed of seven α-helices, forming a transmembrane channel-like structure. The channel is divided into a cytoplasmic (CP) and an extracellular (EC) half-channels, separated

by the chromophore retinal, which is bound through the Schiff base to Lys-242 (12). The crystal structure revealed that Cl[−] interacts with the proton of the protonated Schiff base and the hydroxyl group of Ser-115, as well as the hydrophobic methyl group of Thr-111. The crystal structure also indicated that Cl[−] is hydrated by a cluster of three water molecules that form hydrogen bonds with neighboring amino acid residues. It is noteworthy that anion binding is observed in the crystal structure only at this position of the EC channel, implying that Cl[−] is translocated to the cytoplasmic space by the photon (12). It is assumed that a Cl[−]-binding or -interacting site in the cytoplasmic channel is also required for the release of the translocated Cl[−] into the cytoplasmic space.

Based on the crystal structure, as well as the kinetic analysis, of photoinduced intermediates, the vectorial transport of Cl[−] via HR is composed of three main processes (6,9,11,12,14): 1), Cl[−] binding to the vicinity of the protonated Schiff base region of the retinal chromophore (the EC binding site); 2), Cl[−] translocation; and 3), Cl[−] release from the CP binding site. Investigation of the electrophysiological features of HR pump activity is very important for a better understanding of the function of the pump at the molecular level. The functional activity of HR has been studied using different experimental approaches (1,5,15–19). The function of HR as an inward-directed Cl[−] pump has been clarified with cell envelope vesicles from *H. salinarum*,

Submitted July 13, 2006, and accepted for publication December 5, 2006.

Address reprint requests to Seiji Miyauchi, PhD, Graduate School of Pharmaceutical Sciences, Hokkaido University, Sapporo, Japan 060-0812. E-mail: miya@pharm.hokudai.ac.jp.

© 2007 by the Biophysical Society

0006-3495/07/04/2559/11 \$2.00

doi: 10.1529/biophysj.106.093153

as well as with intact bacteria (1,5,20). Spectroscopic and flux measurements under conditions of different membrane potential have been done with vesicles or bacteria, but these were difficult experiments since precise analysis of voltage dependence is difficult to study with these systems owing to the small size of the bacteria or membrane vesicles. Direct electrical measurements have been undertaken with HR membrane sheets capacitatively coupled to black lipid membranes (15) or to thin films (16–18), and also with membrane suspensions (19). The latter system has an inherent drawback because the orientation of HR cannot be controlled well. Thus, details of the electrophysiological aspects of the Cl^- pump activity of HR are still lacking.

In this study, we used the *Xenopus laevis* oocyte expression system to elucidate the electrophysiological features of *N. pharaonis* halorhodopsin (pHR). In this system, the photoinduced currents due to anion transport could be determined precisely to analyze the kinetics of the transport process. Here, we demonstrate that the Cl^- pump activity via pHR is dependent on membrane potential. Based on this voltage dependence, we show for the first time that the value of reversal potential (V_R) at which the pump current by pHR becomes zero is an intrinsic property of the pump independent of light intensity. These studies also show that the Cl^- pump activity by pHR can generate a considerable negative membrane potential (~ -400 mV), indicating that pHR is a highly active Cl^- pump.

MATERIALS AND METHODS

Construction of the expression plasmid of the histidine-tagged pHR in the oocyte expression vector pGH19

The pGH19 vector (kindly provided by Dr. Peter S. Aronson, Yale University School of Medicine) contains the 3'- and 5'-untranslated regions of the *Xenopus* β -globin gene on the downstream and upstream sides, respectively, of the cloning site. The coding region of pHR was amplified by polymerase chain reaction using the primers 5'-GATATATAGCCATGACTGAGACATTGCCACC-3' (sense) and 5'-TAAGCTTCAGTGGTGGTGGTGGTGGTGGTCCAGGTCGTCAGCGGGAGTGC-3' (antisense), and pET21c(+)-pHR plasmid (21) as the template. A *Hind*III site (underlined residues) was added to the 5'-end of the antisense primer for the purpose of subcloning. The polymerase chain reaction product was first subcloned in a pGEM-T vector (Promega, Madison, WI), and the confirmation of its complete sequence was carried out with the Taq DyeDeoxy terminator method, employing an automated Applied Biosystems 377 Prism DNA sequencer (PerkinElmer, Foster City, CA). The insert was then released by *Eco*RI/*Hind*III double digestion. The pGH19 vector was linearized with *Eco*RI/*Hind*III and then used for the ligation of the pHR cDNA. The resultant product was partially sequenced to confirm the orientation of the insert. The mutant plasmid for the expression of R123K pHR was constructed with a Quickchange site-directed mutagenesis (Stratagene Cloning Systems, San Diego, CA), as described previously (14). The mutation introduced into the plasmid was also confirmed by sequencing.

Functional expression of the histidine-tagged pHR in *Xenopus laevis* oocytes

The amplified pHR cDNA was expressed heterologously in *Xenopus* oocytes by cRNA injection. Capped cRNA was synthesized using

mMESSAGE mMACHINE kit (Ambion, Austin, TX). Mature oocytes (stage V–VI) from *Xenopus* were isolated by treatment with collagenase (1.6 mg/ml), manually defolliculated, and maintained at 18°C in modified Barth's medium, supplemented with 3 μM retinal and 50 $\mu\text{g}/\text{ml}$ gentamicin, as described previously (22,23). On the following day, oocytes were injected with 50 ng pHR cRNA in a 50 nl volume and incubated for 3–5 days. The oocytes were used for electrophysiological studies 3–5 days after cRNA injection. Electrophysiological studies were performed with the two-electrode voltage-clamp (TEVC) technique, as described previously. The oocyte was superfused with perfusion buffer (96 mM NaCl, 2 mM KCl, 1 mM MgCl_2 , 1 mM CaCl_2 , 10 mM Hepes, and 6 mM Tris, pH 7.5). After the current stabilized, the oocyte was superfused with the uptake buffer. The oocyte was voltage-clamped at -50 mV. The composition of the uptake buffer was 2 mM Kgluconate, 1 mM $\text{Mg}(\text{gluconate})_2$, 1 mM $\text{Ca}(\text{gluconate})_2$, 10 mM Hepes, and 100 mM sodium salt (NaCl, NaBr, NaI, NaSCN, NaNO_3 , or sodium 2-(N-morpholino)ethanesulfonate (NaMes)), pH 7.5. The current-voltage (I-V) relationship was analyzed immediately before and within a few seconds after illumination with green light (530 ± 18 nm) when the current reached the maximum and steady state. The green light was produced by a light-emitting diode, Luxeon V Star (Lumileds Lighting, San Jose, CA). The measurements of currents at different membrane potentials were made using short pulses (100 ms) in the range of -150 mV to $+50$ mV in 20-mV increments. Each pulse was separated with a pause (250 ms). TEVC experiments were performed with a TEVC amplifier CEZ-1250 (Nihon Kohden Industry, Tokyo, Japan) and a commercially available program (Clampex software, Axon Instruments, Foster City, CA). The photoinduced current at each applied voltage was calculated as the difference between the steady-state currents recorded before and after illumination. Saturation kinetics of photoinduced currents associated with the anion pump activity was analyzed with seven different concentrations of NaX ($X = \text{Cl}^-$, Br^- , NO_3^- , SCN^- , and I^-). The light-induced currents are defined by kinetic parameters I_{max} (the maximal photoinduced current) and $K_{0.5}$ (the anion concentration necessary for the induction of half-maximal current). Data for the photoinduced current (I) were fitted to the following Michaelis-Menten equation, describing a single saturable component, by an iterative nonlinear least-squares method (Origin, MicroCal, Northampton, MA):

$$I = \frac{I_{\text{max}}[s]}{K_{0.5} + [s]}, \quad (1)$$

where $[s]$ is the concentration of the transportable anion in the perfusion buffer.

Protein expression and purification of the histidine-tagged pHR

The experimental details for protein expression and purification employing *Escherichia coli* BL21(DE3) cells have been described in a previous article (21). Fractions of the proteins using Ni-NTA agarose (Qiagen, Hilden, Germany) were collected by elution (flow rate, 56 mL/h) with buffer E (50 mM Tris-HCl (pH 7.0), 300 mM NaCl, 150 mM imidazole, and 0.1% *n*-dodecyl β -D-maltopyranoside (dodecyl maltoside (DM)) (Dojindo Lab, Kumamoto, Japan)). The yield of the recombinant pHR was almost the same as that reported previously (21).

Flash photolysis spectroscopy

The photocycle of pHR was analyzed by flash spectroscopy with a computer-controlled flash-photolysis apparatus for measuring transient absorption changes every 0.5 μs in the time range from 10 μs to 220 ms. The computer-controlled flash-photolysis apparatus was constructed as described previously (14). The absorbance of the sample in 50–1000 mM NaCl (containing 10 mM MOPS (pH 7.0) and 0.1% DM) was 0.5 at the absorption maximum, and the temperature was maintained at 20°C.

Data analysis of photocycling

The data collected at all wavelengths from 410 to 710 nm were fitted to a multiexponential equation. Singular value decomposition analysis of the observed data confirmed the existence of four kinetically distinguishable photoinduced intermediates (14). The spectrum of the i th-intermediate, P_i , and its decay time constant, τ_i , were calculated according to the Chizhov and Engelhard method (11,14).

RESULTS

Induction of photoinduced outward currents by Cl^- and other anions in *pHR*-expressing *Xenopus* oocytes

The photoinduced currents were monitored under voltage-clamp conditions in oocytes 3–5 days after microinjection of *pHR* cRNA. When *pHR*-expressing oocytes were illuminated with green light ($\lambda_{\text{max}} = 530 \pm 18$ nm) from the light-emitting diode, the presence of Cl^- in the perfusion buffer induced marked outward currents (Fig. 1). Similar currents were also observed with other anions, such as Br^- and I^- , NO_3^- , or SCN^- . These currents were, however, specific since the substitution of Cl^- with Mes^- failed to induce detectable currents. Uninjected oocytes and oocytes injected with water did not show photoinduced currents in the presence of Cl^- with or without incubation of the oocytes with retinal (data not shown). These data demonstrate that *pHR* is able to transport Cl^- , Br^- , I^- , NO_3^- , and SCN^- , and that the transport process is associated with the induction of outward currents. Outward currents in oocytes under voltage-clamp conditions indicate the transfer of negative charges into the oocytes, suggesting that *pHR*-mediated entry of Cl^- and

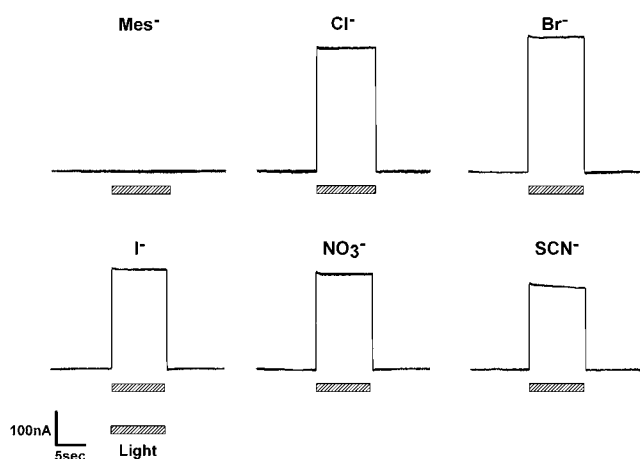


FIGURE 1 Traces of representative currents photoinduced via *pHR* expressed heterologously in *pHR*-expressing *Xenopus* oocytes were superfused with standard buffer containing different anions (as sodium salts) at a concentration of 100 mM. The hatched bars below the current traces indicate the period (10 s) of illumination with green light (530 ± 18 nm). In control oocytes with no *pHR* expression, there were no detectable currents in response to light pulses (data not shown).

other anions into the oocytes is responsible for the outward currents. It is known that *pHR* transports not only Cl^- and other halides (Br^- and I^-) but also NO_3^- and SCN^- (5,24–26). Our electrophysiological data with *pHR*, expressed heterologously in *Xenopus* oocytes, confirm these earlier observations.

Voltage dependence and V_R for *pHR*-mediated anion pump activity

We then characterized the anion pump activity of *pHR* by using the photoinduced anion-dependent outward currents as the readout of the activity. Fig. 2 summarizes the I-V relationship and anion-dependent photoinduced currents at -50 mV. The I-V curve showed linearity in the measurable range of membrane potential (from -150 mV to $+50$ mV) (Fig. 2 A). At -50 mV, the order of the anion-dependent current induced by photons is $\text{Cl}^- = \text{Br}^- > \text{I}^- > \text{NO}_3^- > \text{SCN}^-$ (Fig. 2 B). The I-V relationship data were extrapolated to determine the x -intercepts (i.e., zero current), which correspond to the reversal potentials for different anions. The values for V_R for different anions ranged from -250 mV to -450 mV (Fig. 2 C): The V_R for Br^- is the most negative, followed by that for Cl^- and I^- .

The voltage dependence of the photoinduced current via *pHR*-mediated Cl^- transport was determined at different light intensities (Fig. 3). The magnitude of the photoinduced and Cl^- -dependent currents via *pHR* was linear with light intensity initially but began to plateau subsequently (Fig. 3 A). The profile of the curve indicated that the transport of Cl^- is driven by a single-photon reaction and that the steady-state current is proportional to the excited *pHR* molecule. The slope of the lines describing I-V relationship increased as the light intensity increased (Fig. 3 B). The x -intercept values were similar (~ -400 mV) at all light intensities tested, showing that the V_R is independent of light intensity and that this value represents an intrinsic characteristic of the excited *pHR* molecule. This is further substantiated by the significant change in V_R for the Arg-123 (R123K) mutant (Fig. 4). Arg-123 is critical for Cl^- recognition and transport, and when this amino acid is mutated, it changes the Cl^- pump activity and the V_R . Taken collectively, the data show that the Cl^- pump activity of *pHR* is robust and that the pump can theoretically generate a large negative membrane potential (~ -400 mV) in the presence of extracellular Cl^- .

Kinetics of photoinduced currents associated with *pHR*-mediated Cl^- pump activity

Employing Cl^- as the substrate, we analyzed the saturation kinetics of photoinduced currents in *pHR*-expressing oocytes. The relationship between the photoinduced current and Cl^- concentration at different membrane potentials is described in Fig. 5. The photoinduced outward currents were saturable with increasing concentrations of Cl^- at all

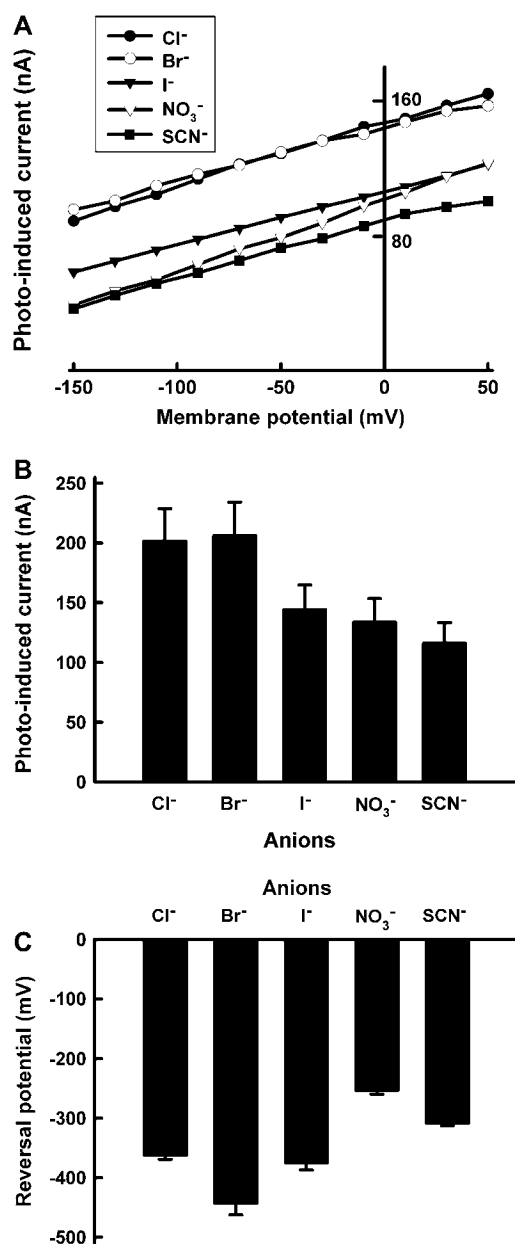


FIGURE 2 Substrate specificity of *pHR*. (A) Representative current-voltage relationship (I-V curve) at steady state for *pHR*-mediated photoinduced currents in the presence of different anions (as sodium salts) (100 mM). (B) Outward photoinduced currents at -50 mV in the presence of various anions. The concentration of anions (as sodium salts) in the perfusion medium was 100 mM. (C) Reversal potentials for the anion pump activity of *pHR* with different anions. The I-V relationship was linear for all anions tested. Reversal potentials were estimated from the *x*-intercepts (i.e., zero current) with the extrapolation of the lines describing the I-V relationship. Data represent mean \pm SE ($n = 4-6$).

membrane potentials examined. The inset in Fig. 5 shows the Eadie-Hofstee plot at a membrane potential of -50 mV. The kinetic parameters were calculated by fitting data to Eq. 1; estimated values were $K_{0.5}$ (concentration of Cl⁻ needed for the half-maximal photoinduced current) = 24.0 ± 2.5 mM

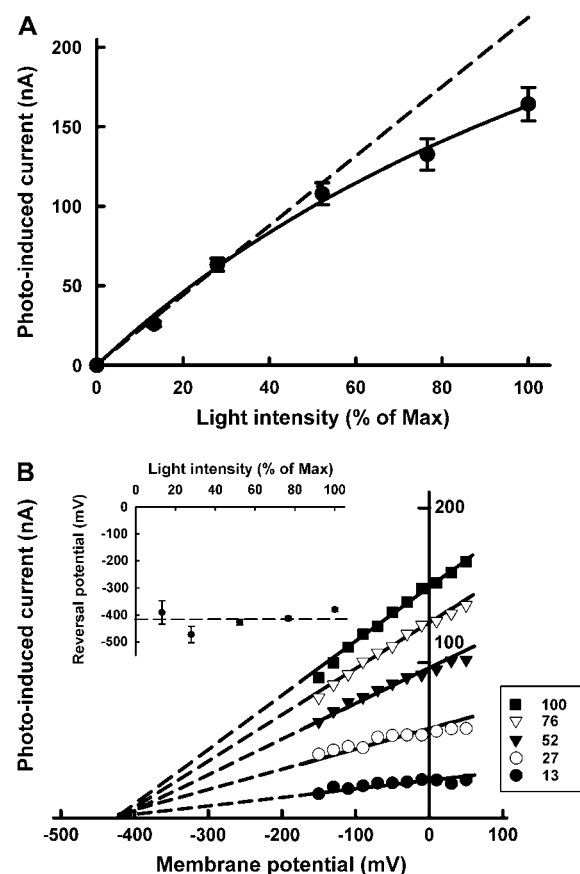


FIGURE 3 Relationship of the Cl⁻ pump activity of *pHR* to light intensity (A) and membrane potential (B). The photoinduced currents in the presence of 100 mM Cl⁻ were determined at steady state in *pHR*-expressing oocytes at different light intensities. The light intensity was measured with a photometer and expressed as percentage of maximal light intensity. (A) The dependence of photoinduced current at -50 mV on light intensity. (B) The dependence of photoinduced current on membrane potential at different light intensities. The V_R was estimated from the *x*-intercepts by the extrapolation of the lines describing the I-V relationship. The reversal potentials remained unchanged irrespective of the light intensity. The inset in B represents the dependence of V_R on light intensity. Data represent mean \pm SE ($n = 7-10$).

(mean \pm SE) and I_{max} (maximal photoinduced current) = 324 ± 22 nA (mean \pm SE). Under the conditions employed in these studies, the dissociation constant of *pHR* for Cl⁻ is thus estimated to be ~ 25 mM. Similar experiments were conducted with other anions recognized by *pHR* and kinetic parameters were calculated for each of them (Table 1). The order of the reciprocal of $K_{0.5}$ value reflecting a binding affinity of anion is: Br⁻ > I⁻ > Cl⁻ > SCN⁻ > NO₃⁻. The $K_{0.5}$ value seems to be related to the size of the hydrated anions. The order of I_{max} value is: Cl⁻ > Br⁻ > I⁻ > NO₃⁻ > SCN⁻.

The dependence of the kinetic parameters, $K_{0.5}$ and I_{max} , on membrane potential is described in Fig. 6. The I_{max} decreased as the membrane potential became more negative, indicating that the rate-determining process in *pHR*-mediated

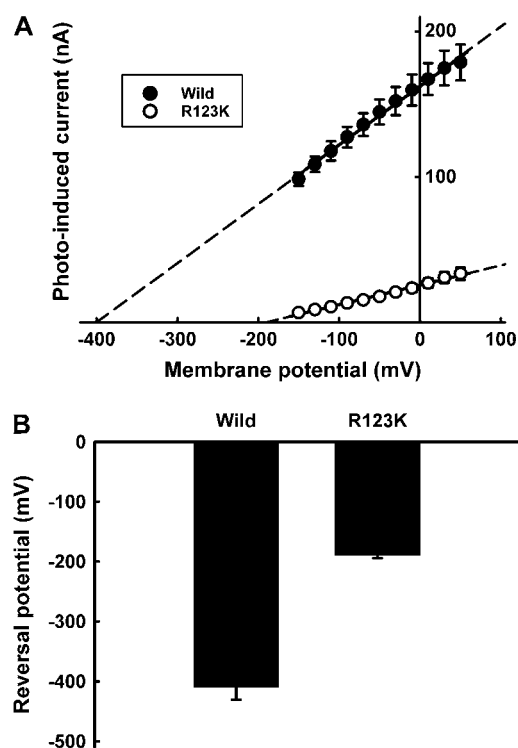


FIGURE 4 Reversal potentials for wild-type and mutant (R123K) *pHR*s. (A) Representative I-V curve at steady state for wild-type and mutant (R123K) *pHR*s. The concentration of Cl^- in the perfusion medium (as NaCl) was 100 mM. (B) Reversal potentials for wild-type and mutant (R123K) *pHR*s. The values were determined from the x -intercepts by the extrapolation of the lines describing the I-V relationship. Data represent mean \pm SE ($n = 6$).

Cl^- transport is dependent on membrane potential. The $K_{0.5}$ also showed marked changes when membrane potential was altered. The value increased markedly as the membrane potential became more negative, implying that the apparent affinity for Cl^- decreased at more negative membrane potentials.

The photocycle of *pHR* with varying Cl^- concentrations

To evaluate the Cl^- -dependent and the rate-determining processes during the photocycle reaction, we analyzed the photocycle of *pHR* at different concentrations of Cl^- (0.05–1 M). The absorbance values observed at different wavelengths (410–710 nm) were fitted simultaneously with four exponentials, since singular value decomposition analysis and the calculation of standard deviation demonstrated the existence of four intermediates. The spectra of the kinetically distinguishable photoinduced intermediates were given in Fig. 7 A. The spectra of P_1 and P_2 were almost the same, and the absorption maximum (λ_{max}) was ~ 520 nm, whereas the spectrum of P_4 showed the same absorption maximum as the original pigment. The profiles of P_1 , P_2 , and P_4 intermediates

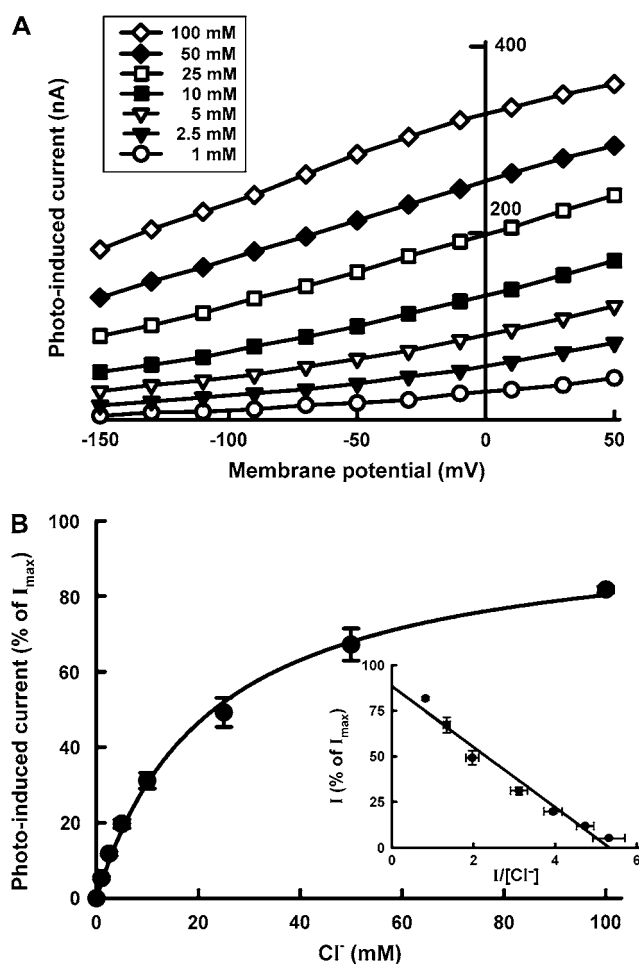


FIGURE 5 Saturation kinetics of the photoinduced Cl^- pump activity of *pHR*. (A) Representative I-V curve at steady state in *pHR*-expressing oocytes at increasing concentrations of Cl^- (as NaCl) (1–100 mM). (B) Photoinduced currents at -50 mV indicative of Cl^- entry as a function of Cl^- concentration. The experiment was repeated five times with different oocytes. Since the expression levels of *pHR* varied among the oocytes, data were normalized by the value of I_{max} , calculated using Eq. 1, in each oocyte. The inset shows the Eadie-Hofstee plot. The $K_{0.5}$ and I_{max} values calculated with a Michaelis-Menten-type equation (Eq. 1) were 24.0 ± 2.5 mM and 324 ± 22 nA, respectively. Data represent the mean \pm SE ($n = 5$).

were independent of Cl^- concentration. The decay time constants (τ_1 and τ_2) were also independent of Cl^- concentration (Fig. 7 B). The P_1 and P_2 intermediates are identified as L_1 and L_2 intermediates, respectively, as indicated by the spectral profile and the decay time constants. Judging from the spectra and the extremely long time constant, the P_4 intermediate is identified as *pHR'* intermediate. On the other hand, the spectra of P_3 intermediate had two absorption maxima, implying that P_3 is comprised of at least two physically defined intermediates that attain equilibrium promptly. Only the P_3 spectrum revealed large Cl^- dependence where considerable shift of the equilibrium occurs from one intermediate with λ_{max} at ~ 610 nm to the other with λ_{max} at ~ 510 nm. The intermediate with λ_{max} at

TABLE 1 Kinetic parameters for anion transport via *pHR* in the voltage-clamped oocytes at -50 mV

Ion	Kinetic parameters	
	$K_{0.5}$ (mM)	I_{\max} (nA)
Cl^-	24.0 ± 2.5	324 ± 22
Br^-	11.2 ± 1.3	280 ± 27
I^-	17.2 ± 1.3	243 ± 20
NO_3^-	45.5 ± 3.8	193 ± 21
SCN^-	27.4 ± 2.0	160 ± 19

The photoinduced currents indicating anion transport rates at -50 mV were determined with increasing concentrations of the anion substrates (1–100 mM). The experiment was repeated with five oocytes. The values for $K_{0.5}$ and I_{\max} were calculated with a Michaelis-Menten-type equation (Eq. 1). Data represent the mean \pm SE ($n = 5$).

~ 610 nm can be thought to be Cl^- -free, because the λ_{\max} value is attributed to a Cl^- -free environment of the protonated Schiff base (21,24,26). Váró et al. (9,10) and Chizhov and Engelhard (11) also described the fast equilibrium between anion-bound and anion-free states in the photocycle. The shift of equilibrium in the P_3 intermediate with changes in Cl^- concentration means that this interme-

diate is involved in the interaction between Cl^- and *pHR*. The decay time constant (τ_3) decreased markedly as Cl^- concentration increased. Judging from the photocycle sequence and the acceleration of the transition rate from P_3 to P_4 (*pHR'*) by the external Cl^- , we conclude that the transition is involved in the Cl^- binding process. Váró et al. (9,10) also demonstrated that the process of Cl^- binding to *pHR* becomes faster as the external Cl^- concentration is increased.

DISCUSSION

In this article, we report on the successful expression of functional *pHR* in *Xenopus laevis* oocytes for electrophysiological characterization of its anion pump activity. This has allowed us to carry out a detailed analysis of the photoinduced anion-dependent outward currents associated with *pHR*-mediated entry of anions into the oocyte. As can be seen in Fig. 1, photoinduced outward currents were detectable only in *pHR*-expressing oocytes when the oocytes were superfused with anions such as Cl^- . Substrate specificity studies showed that *pHR* can recognize and pump a variety of anions, including not only monoatomic (e.g., Cl^- , Br^- , and I^-) but also polyatomic (e.g., NO_3^- and SCN^-) anions. These data are in accordance with those reported previously (5,24,26). The photoinduced currents showed saturation kinetics with all anions that were transported via *pHR*. Duschl and Lanyi have also determined the Cl^- transport activity via *pHR*, employing envelope vesicles from *N. pharaonis* (5). The concentration dependence of Cl^- transport activity by *pHR* followed the Michaelis-Menten-type kinetics, with a single saturable component. The $K_{0.5}$ value for Cl^- reported by Duschl and Lanyi was 25 mM, consistent with the data presented here. The $K_{0.5}$ value, which approximates the dissociation constant for the interaction of the transporter with its substrate, was determined for five different anions (Table 1). Based on these data, the rank order of substrate affinity is as follows: $\text{Br}^- > \text{I}^- > \text{Cl}^- > \text{SCN}^- > \text{NO}_3^-$. The order of the affinity seems dependent on the size of hydrated rather than dehydrated anions, because there is good correlation between the $K_{0.5}$ value and the reciprocal of the limiting equivalent conductivity (λ^0) of anions in water (Fig. 8 A). In general, the λ^0 value reflects the mobility of ion in water, which is dependent on the Stokes radius of ion. Using the spectroscopic analysis of the binding of different anions to *sHR*, Schobert and Lanyi demonstrated that the binding affinity is related not to the dehydrated radius of the transportable anion, but to the Stokes (i.e., hydrodynamic) radius, which reflects the radius of the hydration shell around the anion (27). On the basis of the crystal structure of *sHR*, the binding pocket of Cl^- is composed of the protonated Schiff base, Ser-115, Arg-108, Asp-215, and Trp-112. It is noted that the anion Cl^- remained partially hydrated by a cluster of three water molecules (12), suggesting that the binding pocket has enough room to accommodate anions with different sizes. This is one

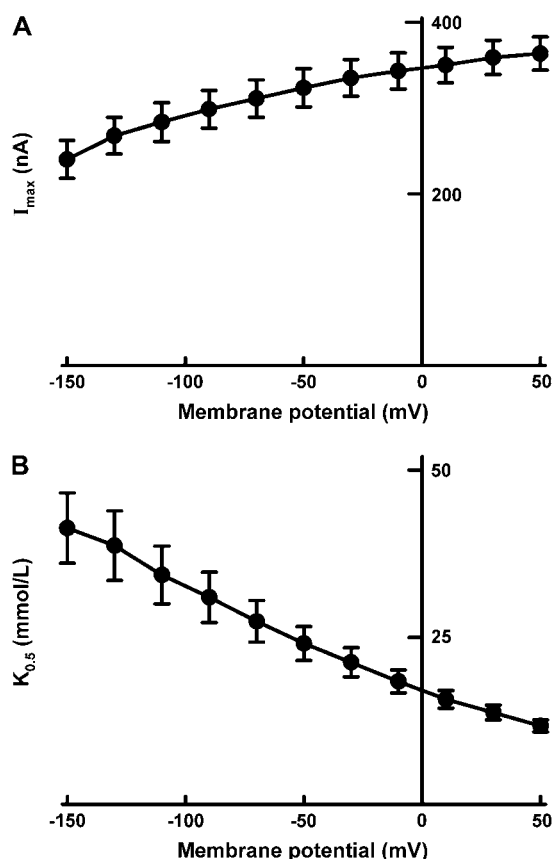


FIGURE 6 Influence of membrane potential on $K_{0.5}$ (i.e., concentration of Cl^- needed for the half-maximal photoinduced current) (A) and I_{\max} (i.e., the maximal photoinduced current at saturating concentrations of Cl^-) (B) in *pHR*-expressing oocytes.

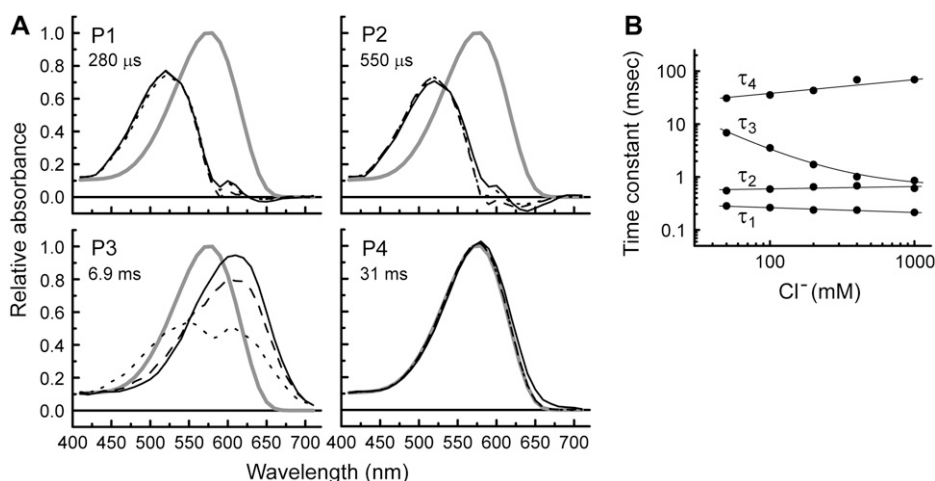


FIGURE 7 Results of the global fitting of the flash-photolysis data of wild-type pHHR. (A) Absorption spectra of unphoto-lyzed (ground) state (P_0) and four kinetically distinguishable intermediates at three representative Cl^- concentrations (solid line, 50mM; dashed line, 400 mM; dotted line, 1000 mM). The P_3 state shows the largest dependence on Cl^- concentration, both in terms of the time constant (τ_3) and the absorption spectrum. The figures represent the time constants corresponding to the states in 50 mM NaCl, pH 7.0, at 20°C. (B) Time constants for the photochemical transitions as a function of Cl^- concentration.

of the reasons why the affinity of anions is dictated by the radius of the hydration shell around the anion. In contrast to the $K_{0.5}$ values, the capacity of the pump activity, I_{\max} , is dependent on the dehydrated sizes of the anions (Fig. 8 B); the rank order of the maximal capacity of the pump activity is as follows: $\text{Cl}^- > \text{Br}^- > \text{I}^- > \text{NO}_3^- > \text{SCN}^-$ (Table 1). These

results suggest that the rate-determining step in the transport cycle shows a dependence on the size of dehydrated ion. Recently, using FTIR spectroscopic analysis data, Shibata et al. demonstrated that the hydrophobicity of the environment in the vicinity of the protonated Schiff base is involved in the translocation of the anion from the EC binding site to the CP binding site (28). The anion might be dehydrated when it is translocated from the EC binding site to the CP binding site (12).

It is interesting to note that the anion pump activity of pHHR shows voltage dependence. The I-V relationship is linear over the range of membrane potential employed (between -150 and +50 mV). The profile of the I-V relationship remains unchanged irrespective of the illumination intensity (Fig. 3). The slope of the I-V curve increased as the number of the excited pHHR molecules increased with the light intensity, whereas the V_R , obtained by the extrapolations of the lines describing the I-V relationship, did not change with different intensities of light. It seems plausible that the slope of the line describing the I-V relationship is a factor of the number of photoexcited pHHR molecules. The linear relationship between photoinduced current and illumination intensity (Fig. 3) demonstrates that the transport of Cl^- via pHHR is driven by a single photon. On the other hand, the value of V_R changed markedly for the mutant of Arg-123 (R123K) (Fig. 4). Since Arg-123 is very critical for the binding and transport of the substrates, the change in V_R as a consequence of mutation of this particular residue suggests that V_R directly reflects the intrinsic ion motive force of the pHHR pump. On the basis of this voltage dependence, we show for the first time that the V_R value at which the pump current is reduced to zero reflects the intrinsic motive force of the excited pHHR molecule to pump Cl^- into the cell. Based on the thermodynamic theory, the Gibbs free energy for the transport of Cl^- by the excited pHHR molecule (ΔG_{imf}) is given by the following equation, since one chloride anion is transported per one photon absorption:

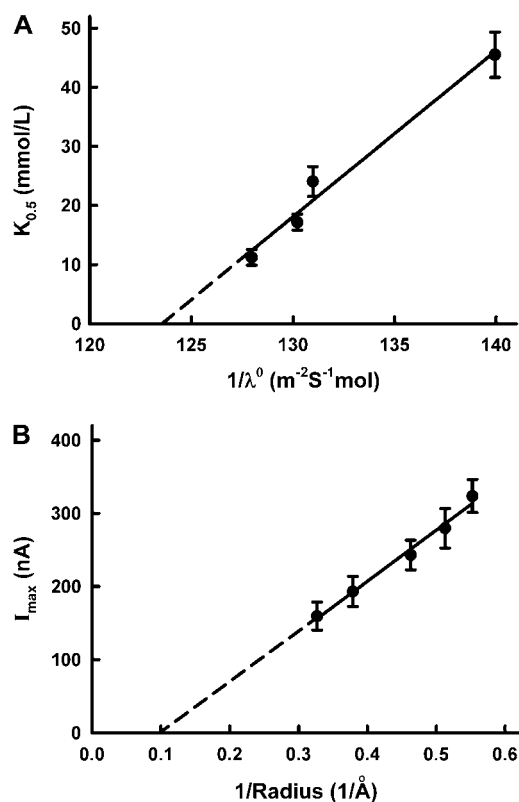


FIGURE 8 Dependence of $K_{0.5}$ on the limiting equivalent conductivities (λ^0) of anions in water (A) and dependence of I_{\max} on the dehydrated radii (B). The values for the limiting equivalent conductivities (λ^0) of anions in water and the dehydrated radii were taken from published reports (33,34).

$$\Delta G_{\text{imf}} = z_i F V_R, \quad (2)$$

where z_i and F represent the valence of the anion and Faraday's constant, respectively. According to Eq. 2, the ΔG_{imf} value was estimated with V_R value -400 mV to be -38.6 (kJ/mol). Employing Planck's constant, the quantum energy for one mole of photon at 580 nm (ΔE_{photon}) is calculated to be 206 (kJ/mol). The probability that $p\text{HR}$ absorbs the light quantum energy, followed by the excitation of $p\text{HR}$, i.e., the isomerization of the retinal from all-*trans* to 13-*cis*, is assumed to be 50%. On the basis of a single photon reaction, the conversion efficiency from the energy of the photon stored in the retinal isomerization to the Cl^- translocation energy is 18.7%.

It has been well characterized that the light-driven pump BR from *H. salinarum* can generate electrochemical potential of up to -280 mV inside the cell (29), which corresponds to a proton motive force to be used for ATP synthesis and is coupled to other secondary active transporters in the plasma membrane. Nagel et al. also estimated the V_R value based on the extrapolation of the line describing the I-V relationship in *Xenopus* oocyte expressing BR to be -220 mV, which is in accordance with the electrochemical potential for protons (30). It should be noted that the Cl^- pumping activity by $p\text{HR}$ can generate a more negative membrane potential, -400 mV, compared with that of BR. The substantial negative V_R of $p\text{HR}$ implies that it is a much more effective anion pump than BR.

As shown in Figs. 2 and 3, the uniqueness of the I-V relationship resides in its linear nature. This raises an interesting question: What is the mechanism for the voltage-dependent change in the anion pump activity of this transporter? In other words, which particular step(s) in the anion pumping via $p\text{HR}$ is (are) regulated by the electric field? The photoinduced current was saturable with respect to Cl^- concentration and followed Michaelis-Menten-type kinetics (Fig. 5). Both $K_{0.5}$ and I_{max} values showed voltage-dependence; the $K_{0.5}$ value increased when the membrane potential became more negative, whereas the I_{max} value decreased. It is of note that the I-V relationship is mainly governed by the voltage-dependent $K_{0.5}$ and I_{max} values. To clarify which step in the photocycle is related to these kinetic parameters with regard to Cl^- pumping, we performed flash-photolysis analysis with different Cl^- concentrations (Fig. 7). In this analysis, we evaluated the rate determining process as well as the Cl^- -dependent processes, for two reasons: 1), all intermediates attain steady state under conditions of continuous illumination, and the excited $p\text{HR}$ consists almost entirely of the population of intermediate molecules in the rate-determining transition; and 2), the photoinduced currents at steady state show Cl^- dependence. It is feasible that a kinetic model describing the photoinduced current at steady state can be simplified, as shown in Fig. 9. Based on these properties of photochemical reaction, we have developed the kinetic model describing the photoinduced current at steady

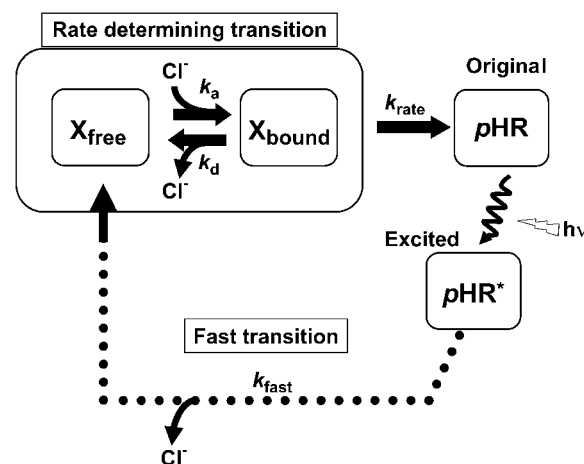


FIGURE 9 A kinetic model for the photoinduced current at steady state for $p\text{HR}$ on the basis of the photocycle. Under conditions of continuous illumination, all intermediates attain steady state, the excited $p\text{HR}$ consists almost entirely of the population of intermediate molecules in the rate-determining transition, and the photoinduced current is governed mainly by the rate determining process. Therefore, focusing only on the intermediates involved in the photoinduced current at steady state, we simplify the photocycle scheme of $p\text{HR}$ and construct the kinetic model describing the photoinduced current due to Cl^- transport via $p\text{HR}$. The kinetic model is comprised of two processes: one is the fast transition of intermediates corresponding to Cl^- translocating and releasing processes, and the other is the rate-determining transition corresponding to Cl^- binding processes. According to the mass conservation, a mass-balance equation consists of the original $p\text{HR}$, the photoexcited $p\text{HR}$ ($p\text{HR}^*$) molecules, and Cl^- free and bound intermediates (X_{free} and X_{bound} , respectively). Taking into consideration that the k_{rate} value is much smaller than any other rate constants (k_{fast} , k_a , and k_d), the photoinduced current at steady state is reduced to Eq. 3.

state (See Appendix and Fig. 9). The scheme is comprised of two processes: one is the fast transition of intermediates corresponding to Cl^- translocating and releasing processes, and the other is the rate-determining transition corresponding to Cl^- binding processes. The photoinduced current is reduced to the following simple equation:

$$I = \frac{k_{\text{rate}} P^* F [\text{Cl}^-]}{\frac{k_a}{k_d} + [\text{Cl}^-]}, \quad (3)$$

where k_a and k_d represent the association and dissociation rate constants, respectively, for Cl^- binding to the EC site, k_{rate} is the rate constant for the rate-determining transition, i.e., the $p\text{HR}' \rightarrow p\text{HR}$ transition, P^* is the $p\text{HR}$ molecule involved in the photoinduced current, and F is Faraday's constant. Analysis of the data using Eq. 3 shows that the voltage dependence of I_{max} is attributed to the $p\text{HR}' \rightarrow p\text{HR}$ transition, which decreased as the membrane potential became more negative. The $K_{0.5}$ value increased as the membrane potential became more negative, implying that the transition decreased, i.e., the association rate decreased and/or the dissociation rate increased as the membrane potential became more negative. Taking the negative charge of Cl^- into account, we hypothesize that during the vectorial

transport of Cl^- there exists an electrical field in the EC channel which affects Cl^- uptake from the EC bulk space.

The binding of various anions has been studied extensively using detergent-solubilized pHR (21,24,26). Based on the absorption wavelength shift caused by the binding of anion to pHR, it has been concluded that the Cl^- binding site has a binding constant of 1–2 mM. Other halides also bind strongly to pHR. On the other hand, the $K_{0.5}$ values reflecting the binding constants of anions in our studies (Table 1) are at least one order of magnitude larger than the binding constants of anions for detergent-solubilized pHR. There are multiple factors that might explain the difference. The kinetic constants for anion binding to detergent-solubilized pHR were determined from the absorption wavelength shift caused by the binding of the anion to the transporter protein (21,24,26). In contrast, we determined the kinetic constants from the photoinduced outward currents associated with the transport of anions via pHR. The binding of the substrate represents only one of multiple steps involved in the transport process. What we determined in our studies is the kinetic constant for the entire transport process rather than for just the binding of the substrate. In addition, membrane potential might have contributed to the differences between the studies. In our oocyte expression system, measurements of pHR function were made in the presence of membrane potential, which induces electrical field in the EC channel of the transporter. According to stopped-flow experiments on the anion binding to detergent-solubilized pHR, Cl^- transport via the transporter occurs mostly by passive diffusion through the EC channel (21). This process is likely to be affected markedly by alterations in the EC channel induced by the electrical field. Furthermore, the binding process of Cl^- is coupled to an electrogenic event in the cycle. If the binding site is not available when the occupancy of an intermediate state at this event is lowered by the external potential, the apparent affinity of the binding will be lowered depending on the membrane potential. It is recognized, however, that the membrane potential provides only a partial explanation of the discrepancy in the kinetic constant values. This is because the value for $K_{0.5}$ is ~ 15 mM when the membrane potential is zero (Fig. 6), and this value is still many times higher than the value obtained with detergent-solubilized pHR. The discrepancy between two experimental systems may also be related to the possibility that Cl^- binds to different states of pHR depending on the experimental system. The binding constant to pHR expressed in *Xenopus* oocytes corresponds to the binding to the intermediate (Fig. 9), whereas the binding constant to detergent-solubilized pHR corresponds to binding to the ground state.

Based on the crystal structure of sHR, the Cl^- binding site is located in the vicinity of the protonated Schiff base, 18 Å below the extracellular membrane surface, i.e., Cl^- is stuck on one-third of its pathway through the membrane (12,13). Supposing that the membrane potential is evenly imposed through the perpendicular vector to the membrane, the

membrane potential from the EC bulk space to the EC binding site is one-third of the whole membrane potential. As shown in Fig. 6, the $K_{0.5}$ value increased almost linearly when the membrane potential was made gradually more negative. Supposing that the increase in $K_{0.5}$ values is governed by the Nernst equation, the imposed membrane potential through the EC channel can be estimated to be 20% of the whole membrane potential. If the membrane potential is -200 mV, the membrane potential of -40 mV might be imposed at least through the EC channel, which corresponds to 60% of the voltage difference in the EC channel theoretically calculated on the basis of the linear membrane potential gradient. In contrast to the formation of the membrane potential gradient through the EC channel in pHR, a hydrogen-bond network is formed through the EC channel in BR, which facilitates movement of the proton through the EC channel. This hydrogen network is believed to be a proton-wire that can rapidly transfer the proton through the EC channel in BR (31,32). Thus, there is no electrical field through the EC channel in BR.

Under conditions of continuous illumination, the photoinduced current attains a steady state. The photoinduced current is governed by the rate-determining step, which is also regulated by the applied electrical field. According to Michaelis-Menten-type kinetics, the I_{\max} value reflects the rate-determining step. On the basis of flash photolysis analysis, the I_{\max} value is a function of the transition rate constant k_{rate} and the photoexcited molecule of pHR. The I_{\max} value reflects the transition of $\text{pHR}' \rightarrow \text{pHR}$, which was estimated to be 10-fold smaller than any other transition in the photocycle. It is important to note that the transition of $\text{pHR}' \rightarrow \text{pHR}$ is also regulated by the applied electrical field. On the basis of the binding analysis of Cl^- to pHR with stopped-flow experiments (21), the time course of the binding to pHR was composed of two phases, indicating that the uptake process of Cl^- through the EC channel is associated with a subtle conformational change or the subtle distortion of the retinal accompanying an intramolecular charge movement. Previously, Manor et al. determined the effect of membrane potential on photochemical reactions of three archaerhodopsins in *H. salinarum*, sensory rhodopsin I, BR, and sHR (20). Each of these three exhibits a decreased rate of thermal decay of the principal photoinduced intermediate when deenergized cells are energized artificially to generate a more negative membrane potential. The intramolecular charge movements with a vectorial component normal to the plane of the membrane possibly occur in the rate-determining thermal steps of each of the three pigments. In other words, a voltage-dependent conformational change common to their respective photocycles might occur. Especially with regard to BR and HR functioning as ion pumps, these conformational movements might be involved in the electrogenic transport associated with the photocycles. Further analysis of this voltage dependence of the rate-determining step might provide a better insight into the

mechanism of the subtle conformational change. The exact mechanism remains yet to be elucidated.

In summary, we have established a *pHR* expression system in *Xenopus laevis* oocytes to gain a better insight into the mechanism of electrogenic anion transport via *pHR*. Using this system, the photoinduced currents due to anion transport could be determined precisely to analyze the kinetics of the transport process. With this approach, we were able to demonstrate that the Cl^- pump activity via *pHR* is dependent on membrane potential. On the basis of this voltage dependence, we show, for the first time that we know of, that the V_R value at which the pump current by *pHR* is reduced to zero represents the intrinsic ion motive force of the excited *pHR* molecule to pump Cl^- into cell. The Cl^- pumping activity by *pHR* can generate a substantial negative membrane potential, -400 mV, i.e., *pHR* functions as a very potent anion pump.

APPENDIX

It has been demonstrated clearly that Cl^- transport into cells via HR is coupled to the cyclic photochemical reaction of HR molecule: all-*trans* to 13-*cis* isomerization of the retinal induced by absorption of a light quantum initiates the photochemical reaction, followed by thermal reisomerization to the initial all-*trans* state. Under conditions of continuous illumination, all intermediates attain steady state and the excited *pHR* consists almost entirely of the population of the intermediate molecules in the rate-determining transition. The photoinduced current is governed mainly by the rate-determining process. The photoinduced current is also dependent on external Cl^- concentration (Fig. 4). Therefore, focusing only on the intermediates involved in the photoinduced current at steady state, we simplify the photocycle scheme of *pHR* and construct a kinetic model describing the photoinduced current due to Cl^- transport via *pHR* (Fig. 9). The kinetic model is comprised of two processes: 1), the fast transition of intermediates corresponding to Cl^- translocating and releasing processes; and 2), the rate determining transition corresponding to Cl^- binding processes. According to the mass conservation, a mass-balance equation consists of the original *pHR*, the photoexcited *pHR* ($p\text{HR}^*$) molecules, and the Cl^- free and bound intermediates (X_{free} and X_{bound} , respectively).

$$\frac{d(A_{\text{pHR}} + A_{\text{pHR}^*})}{dt} = k_{\text{rate}} A_{X_{\text{bound}}} - k_{\text{fast}} A_{\text{pHR}^*}; \quad (\text{A1})$$

$$\frac{dA_{X_{\text{free}}}}{dt} = k_{\text{fast}} A_{\text{pHR}^*} + k_d A_{X_{\text{bound}}} - k_a [\text{Cl}] A_{X_{\text{free}}}; \quad (\text{A2})$$

$$\frac{dA_{X_{\text{bound}}}}{dt} = k_a [\text{Cl}] A_{X_{\text{free}}} - (k_d + k_{\text{rate}}) A_{X_{\text{bound}}}; \quad (\text{A3})$$

where A_{pHR} , A_{pHR^*} , $A_{X_{\text{free}}}$ and $A_{X_{\text{bound}}}$ represent the amounts of original *pHR*, *pHR**, X_{free} , and X_{bound} intermediates, respectively; k_{fast} and k_{rate} are the rate constants with regard to the fast transition and rate-determining transition processes, respectively; and k_a and k_d are the association and dissociation rate constants with regard to Cl^- binding to the EC site in *pHR*. Alternatively, the following equation with regard to the total amount of excited *pHR* molecules involved in the photoinduced current cycle holds as follows:

$$P^* = A_{\text{pHR}^*} + A_{X_{\text{free}}} + A_{X_{\text{bound}}}, \quad (\text{A4})$$

where P^* is the total amount of *pHR* molecules involved in the photoinduced current cycle. Under conditions of continuous illumination,

all intermediates attain steady state and all mass-balance equations described above are equal to zero. Combining all equations, solving of the term, and substituting the value into Eq. A4 yields the following equation:

$$P^* = k_{\text{rate}} A_{X_{\text{bound}}} \left(\frac{1}{k_{\text{fast}}} + \frac{\frac{k_d + k_{\text{rate}}}{k_a}}{k_{\text{rate}} [\text{Cl}]} + \frac{1}{k_{\text{rate}}} \right). \quad (\text{A5})$$

All intermediates attain steady state and all transition rates are equal. Thus, the photoinduced current at steady state is expressed as the multiplicity of $A_{X_{\text{bound}}}$ with k_{rate} and Faraday's constant, F , as follows:

$$I = k_{\text{rate}} F A_{X_{\text{bound}}} = \frac{P^* F}{\frac{1}{k_{\text{fast}}} \frac{k_d + k_{\text{rate}}}{k_a} + \frac{1}{k_{\text{rate}}}}. \quad (\text{A6})$$

Taking into consideration that the k_{rate} value is much smaller than any other rate constants (k_{fast} , k_a , and k_d), Eq. A6 is reduced to

$$I = k_{\text{rate}} F A_{X_{\text{bound}}} = \frac{k_{\text{rate}} P^* F [\text{Cl}]}{\frac{k_d}{k_a} + [\text{Cl}]}. \quad (\text{A7})$$

Substitutions of $k_{\text{rate}} P^* F$ with I_{max} and the ratio $\frac{k_d}{k_a}$ with $K_{0.5}$ yield the Michaelis-Menten-type equation (Eq. 1),

$$I = k_{\text{rate}} F A_{X_{\text{bound}}} = \frac{I_{\text{max}} [\text{Cl}]}{K_{0.5} + [\text{Cl}]}. \quad (\text{A8})$$

The ratio of P^* to the unexcited original *pHR* is designated as α . P^* is expressed as

$$P^* = \frac{\alpha}{\alpha + 1} P_{\text{total}}, \quad (\text{A9})$$

where P_{total} is the total amount of the *pHR* protein expressed in the plasma membrane of *Xenopus* oocyte. Substitution of Eq. A9 into Eq. A7 explains why the photoinduced current is proportional to the intensity of illumination in the range of low intensity, as shown in Fig. 3.

REFERENCES

- Schobert, B., and J. K. Lanyi. 1982. Halorhodopsin is a light-driven chloride pump. *J. Biol. Chem.* 257:10306–10313.
- Mukohata, Y., and Y. Kaji. 1981. Light-induced membrane-potential increase, ATP synthesis, and proton uptake in *Halobacterium halobium*, R1mR catalyzed by halorhodopsin: effects of N,N'-dicyclohexylcarbodiimide, triphenyltin chloride, and 3,5-di-tert-butyl-4-hydroxybenzylidenemalononitrile (SF6847). *Arch. Biochem. Biophys.* 206:72–76.
- Lanyi, J. K. 1990. Halorhodopsin, a light-driven electrogenic chloride-transport system. *Physiol. Rev.* 70:319–330.
- Varo, G. 2000. Analogies between halorhodopsin and bacteriorhodopsin. *Biochim. Biophys. Acta.* 1460:220–229.
- Duschl, A., J. K. Lanyi, and L. Zimanyi. 1990. Properties and photochemistry of a halorhodopsin from the haloalkalophile, *Natronobacterium pharaonis*. *J. Biol. Chem.* 265:1261–1267.
- Rudiger, M., and D. Oesterhelt. 1997. Specific arginine and threonine residues control anion binding and transport in the light-driven chloride pump halorhodopsin. *EMBO J.* 16:3813–3821.
- Lanyi, J. K., A. Duschl, G. W. Hatfield, K. May, and D. Oesterhelt. 1990. The primary structure of a halorhodopsin from *Natronobacterium pharaonis*. Structural, functional and evolutionary implications for bacterial rhodopsins and halorhodopsins. *J. Biol. Chem.* 265:1253–1260.

8. Varo, G., L. Zimanyi, X. Fan, L. Sun, R. Needleman, and J. K. Lanyi. 1995. Photocycle of halorhodopsin from *Halobacterium salinarum*. *Biophys. J.* 68:2062–2072.
9. Varo, G., L. S. Brown, J. Sasaki, H. Kandori, A. Maeda, R. Needleman, and J. K. Lanyi. 1995. Light-driven chloride ion transport by halorhodopsin from *Natronobacterium pharaonis*. 1. The photochemical cycle. *Biochemistry*. 34:14490–14499.
10. Varo, G., R. Needleman, and J. K. Lanyi. 1995. Light-driven chloride ion transport by halorhodopsin from *Natronobacterium pharaonis*. 2. Chloride release and uptake, protein conformation change, and thermodynamics. *Biochemistry*. 34:14500–14507.
11. Chizhov, I., and M. Engelhard. 2001. Temperature and halide dependence of the photocycle of halorhodopsin from *Natronobacterium pharaonis*. *Biophys. J.* 81:1600–1612.
12. Kolbe, M., H. Besir, L. O. Essen, and D. Oesterhelt. 2000. Structure of the light-driven chloride pump halorhodopsin at 1.8 Å resolution. *Science*. 288:1390–1396.
13. Essen, L. O. 2002. Halorhodopsin: light-driven ion pumping made simple? *Curr. Opin. Struct. Biol.* 12:516–522.
14. Sato, M., M. Kubo, T. Aizawa, N. Kamo, T. Kikukawa, K. Nitta, and M. Demura. 2005. Role of putative anion-binding sites in cytoplasmic and extracellular channels of *Natronomonas pharaonis* halorhodopsin. *Biochemistry*. 44:4775–4784.
15. Bamberg, E., P. Hegemann, and D. Oesterhelt. 1984. Reconstitution of halorhodopsin in black lipid membranes. *Prog. Clin. Biol. Res.* 164:73–79.
16. Kalaidzidis, I. V., Y. L. Kalaidzidis, and A. D. Kaulen. 1998. Flash-induced voltage changes in halorhodopsin from *Natronobacterium pharaonis*. *FEBS Lett.* 427:59–63.
17. Okuno, D., M. Asaumi, and E. Muneyuki. 1999. Chloride concentration dependency of the electrogenic activity of halorhodopsin. *Biochemistry*. 38:5422–5429.
18. Muneyuki, E., C. Shibasaki, H. Ohtani, D. Okuno, M. Asaumi, and T. Mogi. 1999. Time-resolved measurements of photovoltage generation by bacteriorhodopsin and halorhodopsin adsorbed on a thin polymer film. *J. Biochem. (Tokyo)*. 125:270–276.
19. Ludmann, K., G. Ibrón, J. K. Lanyi, and G. Varo. 2000. Charge motions during the photocycle of pharaonis halorhodopsin. *Biophys. J.* 78:959–966.
20. Manor, D., C. A. Hasselbacher, and J. L. Spudich. 1988. Membrane potential modulates photocycling rates of bacterial rhodopsins. *Biochemistry*. 27:5843–5848.
21. Sato, M., T. Kanamori, N. Kamo, M. Demura, and K. Nitta. 2002. Stopped-flow analysis on anion binding to blue-form halorhodopsin from *Natronobacterium pharaonis*: comparison with the anion-uptake process during the photocycle. *Biochemistry*. 41:2452–2458.
22. Miyauchi, S., E. Gopal, Y. J. Fei, and V. Ganapathy. 2004. Functional identification of SLC5A8, a tumor suppressor down-regulated in colon cancer, as a Na(+)-coupled transporter for short-chain fatty acids. *J. Biol. Chem.* 279:13293–13296.
23. Gopal, E., Y. J. Fei, M. Sugawara, S. Miyauchi, L. Zhuang, P. Martin, S. B. Smith, P. D. Prasad, and V. Ganapathy. 2004. Expression of slc5a8 in kidney and its role in Na(+)-coupled transport of lactate. *J. Biol. Chem.* 279:44522–44532.
24. Scharf, B., and M. Engelhard. 1994. Blue halorhodopsin from *Natronobacterium pharaonis*: wavelength regulation by anions. *Biochemistry*. 33:6387–6393.
25. Balint, Z., M. Lakatos, C. Ganea, J. K. Lanyi, and G. Varo. 2004. The nitrate transporting photochemical reaction cycle of the pharaonis halorhodopsin. *Biophys. J.* 86:1655–1663.
26. Magyari, K., V. Simon, and G. Varo. 2006. The influence of the halide ions on the photochemical reaction cycle of pharaonis halorhodopsin. *J. Photochem. Photobiol. B.* 82:16–20.
27. Schobert, B., and J. K. Lanyi. 1986. Electrostatic interaction between anions bound to site I and the retinal Schiff base of halorhodopsin. *Biochemistry*. 25:4163–4167.
28. Shibata, M., N. Muneda, T. Sasaki, K. Shimono, N. Kamo, M. Demura, and H. Kandori. 2005. Hydrogen-bonding alterations of the protonated Schiff base and water molecule in the chloride pump of *Natronobacterium pharaonis*. *Biochemistry*. 44:12279–12286.
29. Michel, H., and D. Oesterhelt. 1976. Light-induced changes of the pH gradient and the membrane potential in *H. halobium*. *FEBS Lett.* 65:175–178.
30. Nagel, G., B. Kelety, B. Mockel, G. Buldt, and E. Bamberg. 1998. Voltage dependence of proton pumping by bacteriorhodopsin is regulated by the voltage-sensitive ratio of M1 to M2. *Biophys. J.* 74:403–412.
31. Luecke, H., B. Schobert, H. T. Richter, J. P. Cartailler, and J. K. Lanyi. 1999. Structural changes in bacteriorhodopsin during ion transport at 2 Å resolution. *Science*. 286:255–261.
32. Lanyi, J. K., and H. Luecke. 2001. Bacteriorhodopsin. *Curr. Opin. Struct. Biol.* 11:415–419.
33. Robinson, R. A., and R. H. Stokes. 1959. *Electrolyte Solution*, 2nd ed. Butterworth, London.
34. Israelachvili, J. 1992. *Intermolecular and Surface Forces*. Academic Press, New York.